ARMA 18-826

A bulk damage model for modeling dynamic fracture in rock

Bahmani, B., Abedi, R., Clarke, P.L.
Department of Mechanical, Aerospace & Biomedical Engineering, The University of Tennessee Knoxville/Space Institute, TN, USA

ABSTRACT: The fracture response of rock, as a quasi-brittle material, is highly sensitive to its microstructural design. We present a statistical damage formulation to model dynamic rock fracture. The damage model is rate-dependent and the corresponding damage evolution is a dynamic equation which introduces a timescale to the problem. The introduced timescale preserves mesh objectivity of the method with much less computational efforts in comparison with other conventional non-local formulations. We define a statistical field for rock cohesion to involve microstructure effects in the proposed formulation. The statistical field is constructed through the *Karhunen-Loève* (KL) method. The damage model is coupled with the elastodynamic equation. The final system of coupled equations is discretized by an *asynchronous Spacetime Discontinuous Galerkin* (aSDG) method. Robustness of the proposed formulation is shown though dynamic fracture simulation of rock under uniaxial compressive load. The numerical investigation indicates the importance of load amplitude and microstructure randomness on failure response of rock.
Acknowledgments: The authors gratefully acknowledge partial support for this work via the U.S. National Science Foundation (NSF), CMMI - Mechanics of Materials and Structures (MoMS) program grant number 1538332.

1 INTRODUCTION

Brittle materials have a significant role in various applications: glasses, ceramics, concrete, bone, *etc.* These types of materials are susceptible to sudden rupture by cracking as they have many microdefects and microcracks. Before reaching the ultimate load capacity of a material sample, existing microcracks and microdefects propagate at microscale. At ultimate capacity, microscale degradation processes coalescence and cause fracture initiation at macroscale. Macroscale degradation continues under a softening process until the material completely fails.

An important aspect in fracture of rock, and in general quasi-brittle materials, is the effect of microstructure on their fracture response. As shown in [1] due to the high sensitivity of these materials to their defects, even for the same loading and geometry set-up, different fracture patterns can be observed. Same observations are made in [2] where high variations on material response, especially beyond elastic range—*e.g.,* ultimate load and fracture energy—were observed due to sample to sample variations. *Size effect* is another consequence of the high sensitivity of response to microscale defects, as for example demonstrated in [3, 4]. In fact, the Weibull's weakest link model [5, 6] has proven very effective in capturing the size effect and statistical variation of fracture strength. We have used the Weibull model in the context of an interfacial damage model to capture statistical fracture response of rock, in hydraulic fracturing [7], fracture under dynamic compressive loading [8], and in fragmentation studies [9, 10]. However, as will be discussed below, these models first can become quite expensive due to the use of a sharp interface model for fracture and second are not derived from a homogenization approach.

Sharp interface (SI) models represent fracture on crack surfaces. Some examples include the *linear elastic fracture mechanics* (LEFM) model, cohesive models [11, 12], and interfacial damage models [13–15]. Each of these models has its own advantages/disadvantages. SI models explicitly track real pattern of fractures, but their implementation is cumbersome and their computational cost is high. Also, in applications such as multiscale methods, it is hard to track explicit discontinuities in all scales of interest. If it is even possible, the computation cost will be extremely high. These facts have lead many efforts to develop fracture models based on continuum mechanics.

Bulk/continuum (BC) models use damage mechanics to approximate discontinuous fractures with an equivalent continuum domain. *Smeared crack* approach was formulated in [16] as the earliest BC model to simulate fracture in concrete. Such continuum approaches have several advantages: Simple integration with other numerical methods, fast implementation, and proper utilization in multiscale analyses. The main drawback of BC models is the overestimation of fracture sharpness. Although this issue is not a crucial challenge in many applications, there exists an enhanced type of BC models entitled the *phase field* [17–19] method to recover the sharpness in a continuum fashion.

In dynamics analysis of brittle materials, transient as-

pects of failure mechanism have considerable effects on failure response. Experimental investigations show an increment in load rate increases strength and fracture energy [20,21]. However, most relevant numerical studies are restricted to quasi-static conditions; for example in [22,23] a Weibull model is used to set fracture parameters of a damage model, but the analysis is restricted to static conditions. The lack of study in dynamics conditions leads us to develop an entirely transient formulation for coupled solid-damage mechanisms in rock.

We will use a stochastic approach to model the effects of inhomogeneity and microstructural randomness in dynamic fracture of rock. The use of a bulk damage greatly reduced the computational costs compared to our aforementioned works in the context of an SI model. The use of statistical models for high rates of loading is also motivated by the results in [24] that demonstrate the very poor performance of deterministic models in highly dynamic settings. In the employed stochastic approach, model parameters are statistical fields constructed based on microscale characteristics. In the method proposed here, we construct a realization of the statistical field for rock cohesion based on the well-known *Karhunen-Loève* (KL) method [25,26].

The statistical damage formulation is coupled to elastodynamic equations. As the system of equations is hyperbolic, we use the *asynchronous Spacetime Discontinuous Galerkin* (aSDG) method; this method uses a front-advancing algorithm, called Tent-Pitcher [27] to advance the solution by solving one patch (a small collection of elements) at a time, until the spacetime analysis domain is completely solved. This results in a highly advanced numerical method with local and linear solution properties for the elastodynamic problem [28].

In the following sections, we will describe the proposed damage model and KL method in §2. We will show an application of the method in §3 for a compressive rock sample to indicate the importance of incorporating randomness in dynamics rock fracture. Finally, we will discuss the novel contributions of this study in §4.

2 FORMULATION

In this section, we will focus on new aspects of the proposed formulation. We will introduce the dynamic damage formulation in §2.1 and §2.2. In §2.3, we will express the effect of damage mechanism on the softening behavior of rock. We will indicate the application of the KL method in a statistical analysis in §2.4.

2.1 *Rate-dependent Damage Evolution Law*

In dynamics problems, damage mechanism is not an instantaneous phenomenon. It is more reasonable to take a while for damage mechanism to be entirely activated for material degradation process. The behavior is known as the delay effect in damage initiation and propagation processes. The dynamics damage formulation [13, 29, 30] introduces delay aspects into damage mechanism. A time delay factor (τ_c) is used to derive the evolution equation,

$$\frac{d\kappa}{dt} = \begin{cases} \frac{1}{\tau_c}\left[1 - e^{-a\langle \kappa_f - \kappa \rangle}\right] & \text{if } \kappa < 1 \\ 0, & \text{otherwise} \end{cases} \tag{1}$$

where κ is an internal variable indicating damage level ($0 \leq \kappa \leq 1$), κ_f is the driving force for κ evolution, a is an evolution parameter indicating the brittleness of materials in damage propagation, and $\langle . \rangle$ is Macaulay brackets representing the positive operator.

The damage force term, κ_f, significantly affects the mechanism of damage initiation and propagation. The term should be defined in a proper way to capture characteristic behavior of materials, in terms of their dominant failure modes. There are numerous definitions for κ_f for various applications and material models. We will discuss an appropriate definition of the function for brittle rock materials in the next sub-section.

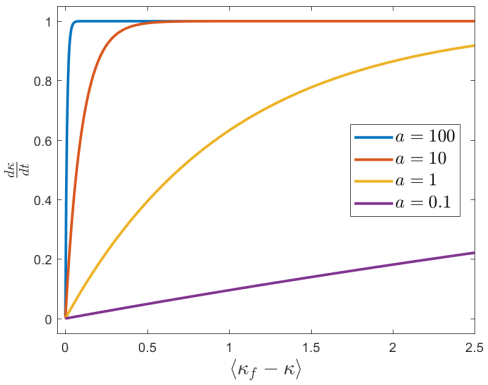

Figure 1: The effect of brittleness coefficient a in the rate of damage evolution. The higher slope shows faster activation of damage mechanism.

Figure 1 shows effect of the brittleness factor, a, in the damage evolution rate. A value equal to 100 represents a highly brittle material behavior, since any damage force value ($\langle \kappa_f - \kappa \rangle$) produces the maximum rate of evolution ($\frac{d\kappa}{dt} = 1$). However, a value equal to 0.1 represents a viscoelastic material behavior, since it takes some time to reach to the entire activation of damage evolution. In the current study, we focus on quasi-brittle materials in rock mechanics applications where a value equal to 10 is a proper selection.

The factor of $\frac{1}{\tau_c}$ in the evolution law Eq. (1) has two essential contributions to remedy some drawbacks of classical damage models. First, it controls damage evolution not to be an instantaneous phenomenon; a higher value of τ_c introduces more delay behavior in the model. Second, the timescale τ_c transforms a local damage formulation to a non-local formulation in spacetime. The non-local behavior preserves the mesh-objectivity of the proposed numerical scheme. The idea is similar to conventional non-local theories for spatial fields (quasi-static behaviors) which are non-localized though a length scale parameter. The delay method is preferable to those type of gradient-based or integration-based non-local methods due to its much less computational and implementation efforts.

2.2 *A Stress-based Damage Model Based on Mohr-Coulomb Failure Criterion*

Two dominant modes of failure in rock are shear and tension. Therefore, it is necessary to utilize a damage model with both sources of the softening behavior. We developed a damage formulation based on the well-known Mohr-Coulomb failure criterion to model shear-tensile degradation of rock.

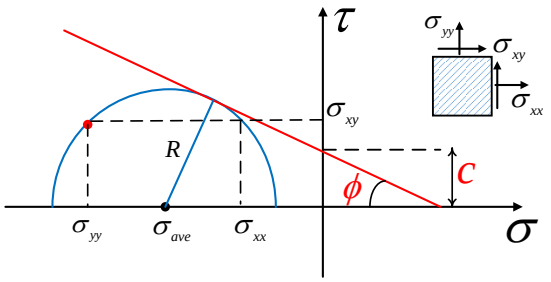

Figure 2: Mohr-Coulomb envelope at a failure stress state.

According to fig. 2 based on the elastic stress tensor $\boldsymbol{\sigma}$, the Mohr-Coulomb failure criterion Y is defied as

$$Y(\boldsymbol{\sigma}, c, \phi) = R + \sigma_{ave}\sin\phi - c\cos\phi \leq 0, \tag{2}$$
$$R = \sqrt{\frac{(\sigma_{xx}-\sigma_{yy})^2}{4} + {\sigma_{xy}}^2},$$
$$\sigma_{ave} = \frac{\sigma_{xx}+\sigma_{yy}}{2},$$

where c and ϕ are material cohesion and internal friction angle, respectively. In the damage model, we define a distance of stress state from the Mohr-Coulomb failure envelope to express the corresponding potential for material degradation as

$$\beta(\boldsymbol{\sigma}, c, \phi) = \frac{R + \sigma_{ave}\sin\phi}{c\cos\phi}, \tag{3}$$

where β shows the tendency in material degradation such that for values $\beta \leq (\underline{\beta} = 1)$ material remains undamaged where $\underline{\beta}$ is the lower limit of damage initiation. Damage values corresponded to $\underline{\beta} < \beta < \bar{\beta}$ indicate non-zero levels of the degradation, and $\bar{\beta}$ is an upper-limit for β to recover the maximum static damage limit. In static analysis, the upper-limit $\bar{\beta}$ corresponds to the maximum damage value $\kappa_{max} = 1$. So, we define the normalized damage force function as

$$\kappa_f = \frac{\beta - \underline{\beta}}{\bar{\beta} - \underline{\beta}}. \tag{4}$$

2.3 *Stiffness Degradation by Damage Value*

The constitutive law of linear elastic materials for undamaged material is

$$\boldsymbol{\sigma} = \mathbf{C}\boldsymbol{\epsilon}, \tag{5}$$

where $\mathbf{C}$ is the fourth order elasticity tensor and $\boldsymbol{\epsilon}$ is the second order linear strain tensor. However, in the case of existing damage, an effective definition of stress tensor ($\boldsymbol{\sigma}_{eff}$) is used in solid deformation analysis to incorporate the corresponding material softening behavior. In our proposed approach, we apply the damage effect on the pure shear and hydrostatic tension parts of the elastic stress tensor to define the effective stress tensor. Accordingly, we first decompose the stress tensor into two parts of *deviatoric* (σ_d) and *hydrostatic* (σ_h) stresses. Then, the effective stress relation will be

$$\boldsymbol{\sigma}_{\text{eff}} = (1-\kappa)\boldsymbol{\sigma}_d + (1-\kappa)\langle\boldsymbol{\sigma}_h\rangle + (\boldsymbol{\sigma}_h - \langle\boldsymbol{\sigma}_h\rangle), \tag{6}$$

where the first term of the right-hand side shows the effect of shear stresses and the second term represents the effect of tensile stresses in material degradation processes. The set of equations 1-6 represents an appropriate continuum damage model to incorporate dynamics and rate effects of the damage evolution into elastodynamics equation.

2.4 *Realization of Stochastic Damage Model Parameters*

Material uncertainty is incorporated into the continuum damage model by treating the isotropic cohesion c parameter as a spatially inhomogeneous random field $c(\mathbf{x}, \omega)$ governed by probability structure ω. Bypassing the derivation of statistics from some "real" material microstructure, the statistical characteristics of the random cohesion field are assumed to follow a certain point-wise statistics and covariance function form. The random field is developed by enforcing a stationary covariance of γ-*exponential* form with prescribed correlation length to control spatial variability of the field. The distribution of the cohesion random field is assumed to follow a log-normal Lognormal(μ, σ^2) probability structure with mean $\exp\left(\mu + \sigma^2/2\right)$ and variance $[\exp(\sigma^2)-1]\exp(2\mu+\sigma^2)$ of the log-normal field as material model input.

Having knowledge of the underlying material statistics, there are a number of methods that allow a scalar random field approximation to be generated wherein the inherent statistics are preserved. On such method is the Karhunen-Loéve (KL) method which approximates a random field $\xi = \xi(\mathbf{x}, \omega)$ by an expansion of its covariance kernel; the field is described by the series,

$$\xi(\mathbf{x}, \omega) = \mu_\xi(\mathbf{x}) + \sum_{i=1}^{n} \sqrt{\lambda_i} b_i(\mathbf{x}) Y_i(\omega), \tag{7}$$

where the denumerable set of eigenvalues λ_i and eigenfunctions $b_i(\mathbf{x})$ are obtained as solutions of the Fredholm equation, *i.e.,* the generalized eigenvalue problem (EVP), which is detailed [31]. Due to the monotonically decreasing property of the eigenvalue solutions, the truncated series with an appropriately chosen n number of terms can precisely represent the statics of the underlying random field while converging to the infinite KL series limit as $n \to \infty$. For practical use of the KL method, the uncorrelated random variables Y_i must also be independent; this is valid only if the random variables and consequently the random field

$\xi(\mathbf{x}, \omega)$ are Gaussian. This Gaussian requirement does not hinder the use of the KL approximated random field as the *inverse transform method* provides a means of transforming one probability structure to another provided the cumulative density function of both distributions are known *a prior*; this mapping is required to transform the KL Gaussian random field approximation to an approximation of the originally assumed log-normal distribution. Please refer to [32] for an overview of the use of KL method in modeling rock fracture strength and [10] for further elaboration on the KL and eigen-pair solution procedures, particularly for non-Gaussian fields.

3 NUMERICAL RESULTS

We show robustness of the proposed method by numerical analyses of a sample rock at different conditions. The sample problem is under a uniaxial pressure loading at its top and bottom edges, as shown in fig. 3. The geometry is a rectangle with $w = 0.08$ mm and $l = 2w = 0.16$ mm. The problem is in the plane-strain condition and material properties are $\rho = 2650$ kg/m^3, $E = 65$ GPa, $\nu = 0.27$, $c = 4.7$ MPa, and $\phi = 17^\circ$ corresponded to density, elastic modulus, Poisson ratio, cohesion and friction angle, respectively. The time scale parameter is chosen equal to $\tau_c = 0.03$. The convergence criterion for the nonlinear solver is based on the system energy norm and the corresponding tolerance is 10^{-8}. We utilize third order polynomial basis functions for damage and displacement fields in time and space axes.

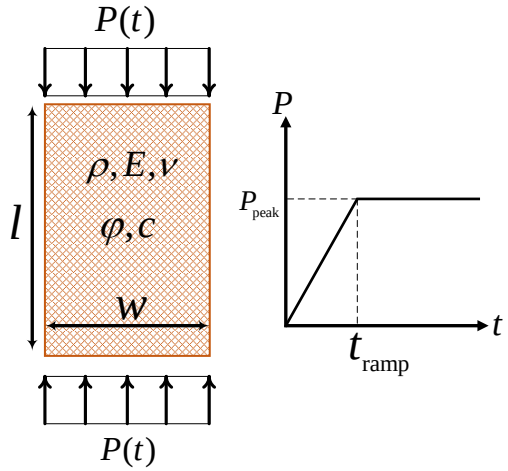

Figure 3: A pressurized sample with the ramp loading at its ends.

The initial computational domains for the simulations consist of three triangular meshes: coarse (8×16), medium (16×32), and fine (32×64). These meshes, fig. 4, are used to construct the spacetime solution manifold in the $\mathbb{E}^2 \times \mathbb{R}$. The time slabs are progressively generated based on wave characteristics to obtain the best achievable performance of the numerical method. The method has the advantage of solving the discrete problem element-wise which is perfect for the parallel processing design.

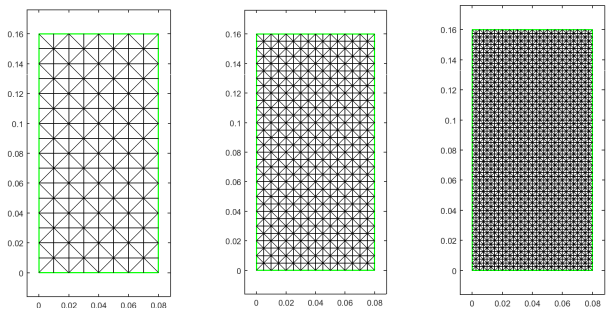

(a) 8×16 (b) 16×32 (c) 32×64

Figure 4: Initial meshes for the simulations: (a) Coarse; (b) Medium; (c) Fine.

In the following cases, the ramp time is $t_{\text{ramp}} = 0.01$ ms and all the physical parameters are constant except load magnitude P_{peak} and material cohesion c. The effect of load magnitude is investigated for two cases of the high load $P_{\text{peak}} = 13.5$ MPa and the low load $P_{\text{peak}} = 6$ MPa. In the study of the effect of randomness and inhomogeneity, the cohesion value is a random field with the mean value equal to the homogeneous case ($c = 4.7$ MPa) and the standard deviation of 2.35 MPa. The random field is a realization based on the KL method with the correlation length equal to 5 mm.

3.1 *Mesh Objectivity*

The sensitivity of elastic and damage results on the resolution of the underlying discrete grid, *i.e.,* mesh sensitivity, is a well-known problem for many bulk damage models. As described before, the proposed damage formulation has an inherent length scale which is coupled by a timescale in dynamics fashion. To show that, we will compare the damage evolution for two different meshes in fig. 5. The chosen meshes are the coarse (fig. 4a) and medium (fig. 4b) meshes. The material properties are homogeneous and loading magnitude is $P_{\text{peak}} = 13.5$ MPa.

The results in fig. 5 indicate that both the meshes represent almost same responses for the damage evolution. There exist two competing factors in the proposed damage formulation in comparing with other mesh objective damage formulations. First, the implementation effort is less than integration-based non-local damage models. Second, the computational cost is less than gradient-based non-local damage formulations.

3.2 *The Effect of Load Amplitude*

We will show that load intensity is one of the critical factors in failure behavior of brittle materials. Again, in this case, the material properties are homogeneous, and we just consider two different load magnitudes.

Figure 6 shows the damage evolution at different times for the low amplitude load. Figure 7 depicts the strain energy of the solid deformation at each corresponding time. In this problem, two symmetric compressive waves travel from top and bottom toward each other in the middle. Before the collision of the two waves, the solid energy is not

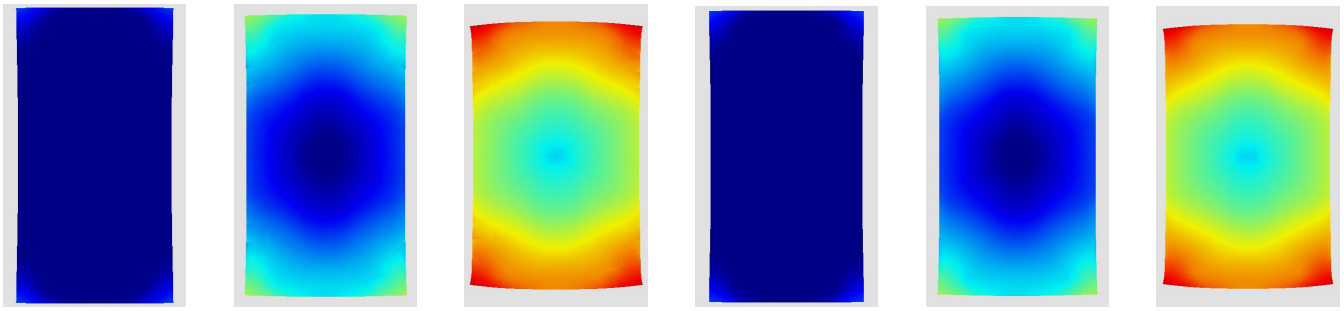

(a) $t = 13.9$ μs (b) $t = 24.7$ μs (c) $t = 36.1$ μs (d) $t = 13.9$ μs (e) $t = 24.7$ μs (f) $t = 36.1$ μs

Figure 5: Damage responses at different times for two different meshes. Figures (a) to (c) correspond to the coarse mesh and figs. (d) to (f) correspond to the medium mesh. The results are shown on the deformed mesh which is magnified by the factor of 300. The values continuously vary from zero (blue color) to unity (red color).

sufficient to produce any damage. However, when these waves collide, they interact and double the stress wave magnitude at the collision area. The increment in the energy causes the damage initiation at the potential zone. Then, the damage zone progresses toward end edges of the sample where the reflected waves travel.

Figures 8 and 9 show the damage and strain energy density results for the high amplitude load case at various times, respectively. For a better comparison, we tried to present these results at time sequences close to the previous case, but as the wave magnitudes and propagation patterns are distinct, presentation of the cases at same time sequences does not clearly illustrate the entire damage mechanism. In the high load condition, the solid energy produces damage earlier than the previous case, before the first collision of the two stress waves in the middle. In this case, almost everywhere is damaged and the pattern of damage evolution is entirely different from the low load condition. The comparison shows how the damage threshold, load amplitude, and transient effects can interact with each other to get more realistic simulations. We will consider the effect of damage threshold (*e.g.,* material cohesion), in the next case study.

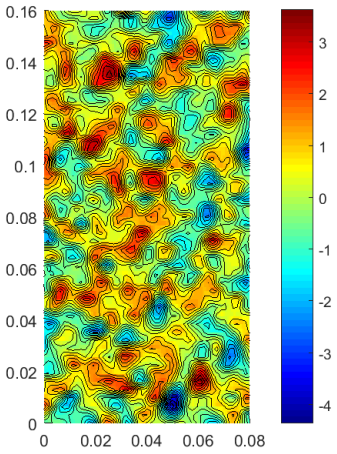

Figure 12: A realization for random distributed cohesion values with the correlation length of 5 mm.

3.3 *The Effect of Randomness*

The homogeneous assumption for brittle materials such as rock is not reasonable as they have many defects and microcracks in their microstructure. Therefore, it is crucial to incorporate these effects in the macroscale analysis to get more reliable results. In this case, we focus on the effect of microstructure on the material cohesion which is one of the most important parameters in the dynamic failure criterion used.

Figure 12 shows a realization of the underlying randomness for the material cohesion of the sample. The realization is constructed with 2000 terms of the KL series. We used a fine mesh to have an adequate resolution for capturing the underlying randomness.

Figure 10 and 11 show damage and strain energy changes at various times, respectively. The simulations are performed for the low amplitude load. The results indicate the significant effect of randomness on elastodynamic and damage field evolution in comparison with the homogeneous condition in fig. 6 and fig. 7. The model performs well to capture weakest points which are consistent with the underlying random field, in fig. 12 weakest zones are distinguishable by the blue color. The statistical damage model is more consistent with SI models. The reason is: First, damage initiation zones are point-wise (same as fracture initiation locations); Second, damaged zones tend to propagate in specific inclined directions rather than diffuse around initiation points (narrower band in comparing with a homogeneous damage model). These failure zones qualitatively match with other numerical and experimental observations [33–37] in that fractures propagate in specific angles, *i.e.,* $\pm(45° \pm \phi/2)$ where ϕ is the friction angle, with respect to the loading direction.

Therefore, as recommended by [9], statistical models in fracture analyses of brittle materials help not only improve the reality of simulations but also remedy some numerical challenges in fracture modeling such as diffusive responses of BC models or instant ruptures of BC/IC models.

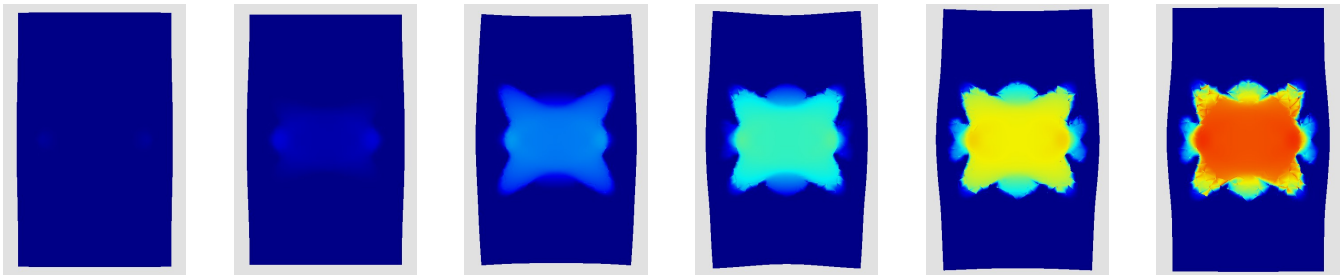

(a) $t = 13.9$ μs (b) $t = 24.7$ μs (c) $t = 36.1$ μs (d) $t = 42.2$ μs (e) $t = 48.2$ μs (f) $t = 53.4$ μs

Figure 6: The damage evolution at various times for the medium mesh at the low load condition. The results are shown on the deformed meshes which are magnified by the factor of 1000. The values continuously vary from zero (blue color) to unity (red color).

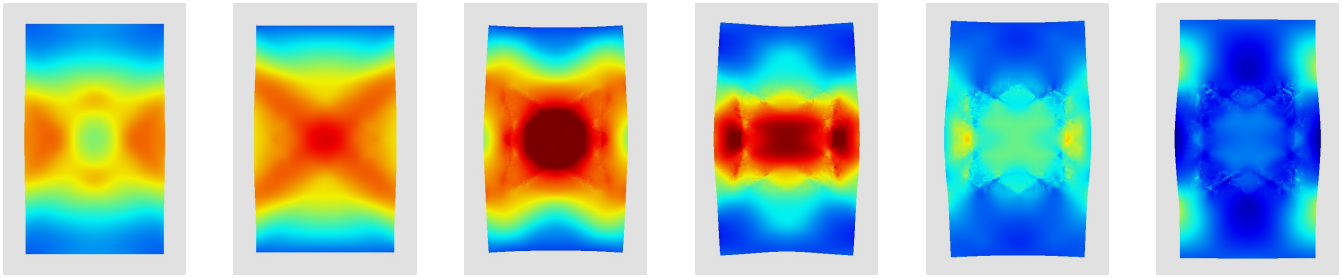

(a) $t = 28$ μs (b) $t = 30.7$ μs (c) $t = 36.7$ μs (d) $t = 42.2$ μs (e) $t = 48.2$ μs (f) $t = 53.4$ μs

Figure 7: The strain energy distribution at various times for the medium mesh at the low load condition. The results are shown on the deformed mesh which is magnified by the factor of 1000. The values continuously vary from zero (blue color) to 2.5×10^{-3} MPa (red color).

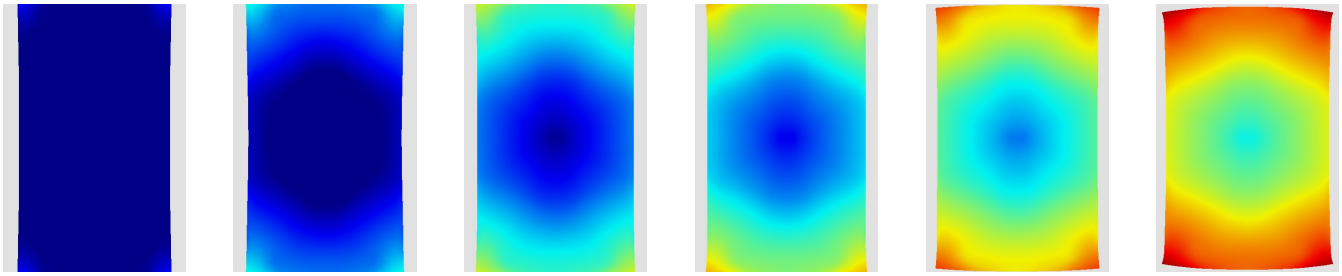

(a) $t = 13.9$ μs (b) $t = 21.1$ μs (c) $t = 26.8$ μs (d) $t = 29.2$ μs (e) $t = 33.2$ μs (f) $t = 37.4$ μs

Figure 8: The damage evolution at various times for the medium mesh at the high amplitude load. The results are shown on the deformed meshes which are magnified by the factor of 300. The values continuously vary from zero (blue color) to unity (red color).

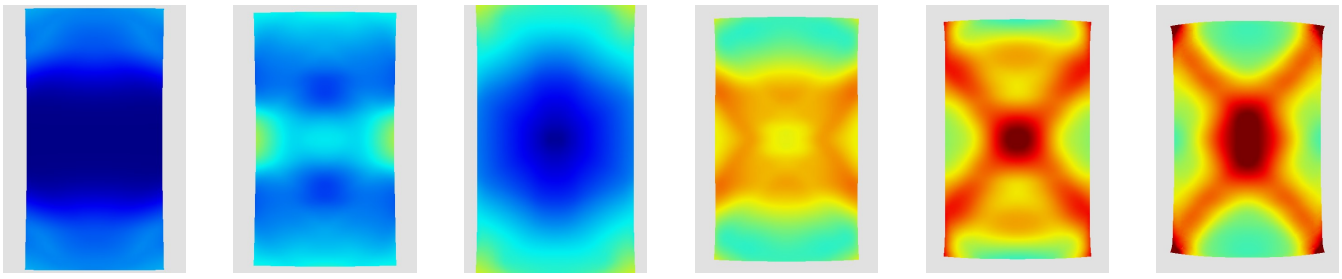

(a) $t = 13.9$ μs (b) $t = 21.1$ μs (c) $t = 26.8$ μs (d) $t = 29.2$ μs (e) $t = 33.2$ μs (f) $t = 37.4$ μs

Figure 9: The strain energy distribution at various times for the medium mesh at the high amplitude load. The results are shown on the deformed mesh which is magnified by the factor of 1000. The values continuously vary from zero (blue color) to 2.5×10^{-3} MPa (red color).

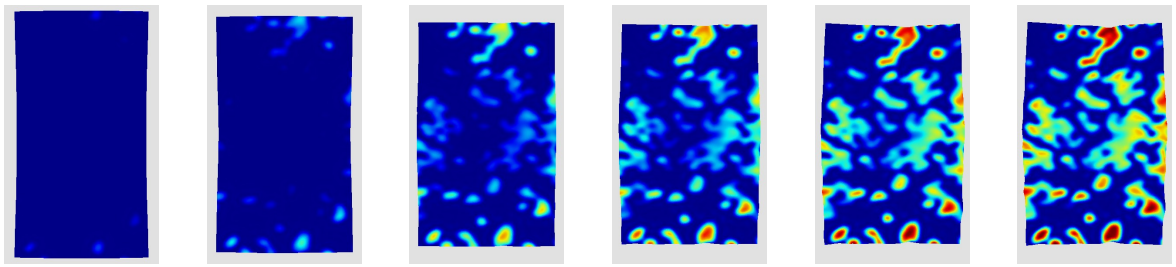

(a) $t = 13.9\ \mu s$ (b) $t = 21.1\ \mu s$ (c) $t = 29.2\ \mu s$ (d) $t = 33.2\ \mu s$ (e) $t = 37.4\ \mu s$ (f) $t = 40\ \mu s$

Figure 10: The damage evolution at various times for a random field of material cohesion with mean value of $c = 4.7$ MPa and standard deviation of 2.35 MPa. The applied load is low. The values continuously vary from zero (blue color) to unity (red color). The deformed mesh is magnified by a factor of 1000.

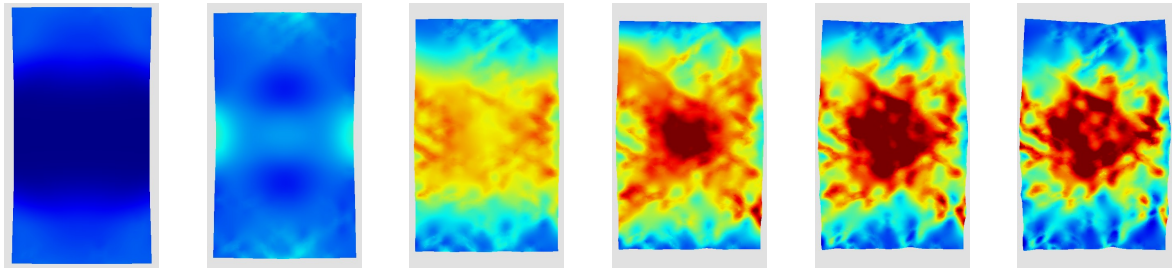

(a) $t = 13.9\ \mu s$ (b) $t = 21.1\ \mu s$ (c) $t = 29.2\ \mu s$ (d) $t = 33.2\ \mu s$ (e) $t = 37.4\ \mu s$ (f) $t = 40\ \mu s$

Figure 11: The strain energy distribution at various times for a random field of material cohesion with mean value of $c = 4.7$ MPa and standard deviation of 2.35 MPa. The applied load is low. The values continuously vary from zero (blue color) to 2.5×10^{-3}MPa (red color). The deformed mesh is magnified by a factor of 1000.

4 CONCLUSIONS

In the current study, we formulated a new damage model for brittle materials with the consideration of tensile and shear failure modes. The transient damage evolution adopted from Allix's model governs the irreversible progress of damage in time. The transient model uses a timescale to introduce the rate-dependency and preserve the mesh objectivity. We proposed a statistical framework through the KL method to include microstructure randomness of the material cohesion in the damage model. The final system of hyperbolic equations is discretized in space and time by the aSDG method. The aSDG method is well-suited for hyperbolic system of equations to track wave shocks precisely with complex meshes in the spacetime. The final system of nonlinear equations is solved with the Newton-Raphson method.

We showed the mesh objectivity of the method for highly dynamic problems. The objectivity comes from the timescale parameter τ_c which is equivalent to the length scale parameter in non-local theories. We studied the effect of load amplitudes in the dynamic damage formulation. The load amplitude has a significant role in the damage mechanism and consequently the failure pattern of brittle materials. The most important factor to get more realistic simulations is the incorporation of microstructure characteristics in brittle materials. The randomness of the material cohesion indicates a dominant effect in the failure pattern of brittle materials. We showed the statistical bulk damage model produces a failure response which is more consistent with interfacial fracture models.

There are a few extensions to the proposed fracture model. First, the main focus in this study was determination of the initial stages of macroscopic failure, *i.e.,* when κ reaches unity in certain regions. In future work, we will apply the same idea in [19] which uses a reduction factor for the damage effect in the mechanical degradation process in Eq. (6). This prevents κ reaching unity and enables the continuation of analysis beyond the stages shown here. Second, in Eq. (6) the effective damage-stage friction coefficient is zero. We will improve the damage model to enable some residual friction coefficient at full damage. This will improve the predicted slip plane angles shown in fig. 10.

In this work, for the statistical analysis we assumed an artificial statistics for rock cohesion. In future works, we aim to use statistical volume elements (SVEs) to homogenize both elastic and fracture properties of rock at different length scales. Beyond the more physical representation of these random fields, similar to [38] we will characterize fracture strength as a function of the angle of loading. This aspect will particularly be important in modeling the effect of bedding planes in rock fracture. In addition, we aim to extend [39] to formulate an h-adaptive scheme in spacetime that simultaneously controls the errors associated with elastodynamic and bulk damage problems.

REFERENCES

[1] A. Al-Ostaz and I. Jasiuk. Crack initiation and propagation in materials with randomly distributed holes. *Engineering Fracture Mechanics*, 58(5-6):395–420, 1997.

[2] J Kozicki and J Tejchman. Effect of aggregate structure on fracture process in concrete using 2D lattice model. *Archives of Mechanics*, 59(4-5):365–84, 2007.

[3] A. Rinaldi, D. Krajcinovic, and S. Mastilovic. Statistical damage mechanics and extreme value theory. *International Journal of Damage Mechanics*, 16(1):57–76, 2007.

[4] M. Genet, G. Couegnat, A.P. Tomsia, and R.O. Ritchie. Scaling strength distributions in quasi-brittle materials from micro- to macro-scales: A computational approach to modeling nature-inspired structural ceramics. *Journal of the Mechanics and Physics of Solids*, 68(1):93–106, 2014.

[5] W. Weibull. A statistical theory of the strength of materials. *R. Swed. Inst. Eng. Res.*, page Res. 151, 1939.

[6] W. Weibull. A statistical distribution function of wide applicability. *Journal of Applied Mechanics*, 18:293–297, 1951.

[7] R. Abedi, O. Omidi, and P.L. Clarke. Numerical simulation of rock dynamic fracturing and failure including microscale material randomness. In *Proceeding: 50th US Rock Mechanics/Geomechanics Symposium*, Houston, Texas, USA, 2016. ARMA 16-0531.

[8] R. Abedi, R.B. Haber, and A. Elbanna. Mixed-mode dynamic crack propagation in rocks with contact-separation mode transitions. In *Proceeding: 51th US Rock Mechanics/Geomechanics Symposium*, San Francisco, California, USA, 2017. ARMA 17-0679.

[9] Reza Abedi, Robert B. Haber, and Philip L. Clarke. Effect of random defects on dynamic fracture in quasi-brittle materials. *International Journal of Fracture*, 208(1-2):241–268, 2017.

[10] P.L. Clarke, R. Abedi, B. Bahmani, K.A. Acton, and S.C. Baxter. Effect of the spatial inhomogeneity of fracture strength on fracture pattern for quasi-brittle materials. In *Proceedings of ASME 2017 International Mechanical Engineering Congress & Exposition IMECE 2017*, Tampa, Florida, USA, 2017. IMECE2017-71515.

[11] D. S. Dugdale. Yielding of steel sheets containing slits. *Journal of the Mechanics and Physics of Solids*, 8:100–104, 1960.

[12] G. I. Barenblatt. The mathematical theory of equilibrium of cracks in brittle fracture. *Advanced Applied Mechanics*, 7:55–129, 1962.

[13] O Allix, P Feissel, and P Thévenet. A delay damage mesomodel of laminates under dynamic loading: basic aspects and identification issues. *Computers & structures*, 81(12):1177–1191, 2003.

[14] Giulio Alfano. On the influence of the shape of the interface law on the application of cohesive-zone models. *Composites Science and Technology*, 66(6):723–730, 2006.

[15] Francesco Parrinello, Boris Failla, and Guido Borino. Cohesive-frictional interface constitutive model. *International Journal of Solids and Structures*, 46(13):2680 – 2692, 2009.

[16] Z. P. Bažant and F. B. Lin. Nonlocal smeared cracking model for concrete fracture. *Journal of Structural Engineering*, 114(11):2493–2510, 1988.

[17] G.A. Francfort and J.-J. Marigo. Revisiting brittle fracture as an energy minimization problem. *Journal of the Mechanics and Physics of Solids*, 46(8):1319 – 1342, 1998.

[18] B. Bourdin, G.A. Francfort, and J-J. Marigo. Numerical experiments in revisited brittle fracture. *Journal of the Mechanics and Physics of Solids*, 48(4):797 – 826, 2000.

[19] C. Miehe, F. Welschinger, and M. Hofacker. Thermodynamically consistent phase-field models of fracture: Variational principles and multi-field fe implementations. *International Journal for Numerical Methods in Engineering*, 83(10):1273–1311, 2010.

[20] LF Pereira, J Weerheijm, and LJ Sluys. A new effective rate dependent damage model for dynamic tensile failure of concrete. *Engineering Fracture Mechanics*, 176(Supplement C):281–299, 2017.

[21] P. H. Bischoff and S. H. Perry. Impact behavior of plain concrete loaded in uniaxial compression. *Journal of engineering mechanics*, 121(6):685–693, 1995.

[22] C.A. Tang, H. Liu, P.K.K. Lee, Y. Tsui, and L.G. Tham. Numerical studies of the influence of microstructure on rock failure in uniaxial compression - part I: effect of heterogeneity. *International Journal of Rock Mechanics and Mining Sciences*, 37(4):555–569, 2000.

[23] WC Zhu, JG Teng, and CA Tang. Mesomechanical model for concrete. part I: model development. *Magazine of concrete research*, 56(6):313–330, 2004.

[24] R. Abedi, O. Omidi, and P.L. Clarke. A numerical study on the effect of loading and randomness on fracture patterns in a tight formation. In *Proceeding: 51th US Rock Mechanics/Geomechanics Symposium*, San Francisco, California, USA, 2017. ARMA 17-0641.

[25] Kari Karhunen and Ivan Selin. *On linear methods in probability theory*. Rand Corporation, 1960.

[26] M. Loéve. *Probability theory*. Springer, New York, 1977.

[27] Reza Abedi, Shuo-Heng Chung, Jeff Erickson, Yong Fan, Michael Garland, Damrong Guoy, Robert Haber, John M. Sullivan, Shripad Thite, and Yuan Zhou. Spacetime meshing with adaptive refinement and coarsening. In *Proceedings of the Twentieth Annual Symposium on Computational Geometry*, SCG '04, pages 300–9, Brooklyn, New York, USA, June 9-11 2004. ACM.

[28] Reza Abedi, Robert B. Haber, and Boris Petracovici. A spacetime discontinuous Galerkin method for elastodynamics with element-level balance of linear momentum. *Computer Methods in Applied Mechanics and Engineering*, 195:3247–73, 2006.

[29] O Allix and A Corigliano. Modeling and simulation of crack propagation in mixed-modes interlaminar fracture specimens. *International Journal of Fracture*, 38:111–140, 1999.

[30] A Corigliano and M Ricci. Rate-dependent interface models: formulation and numerical applications. *International Journal of Solids and Structures*, 38:547–576, 1999.

[31] R. Ghanem and P.D. Spanos. *Stochastic finite elements: a spectral approach*. Springer-Verlag, 1991.

[32] P.L. Clarke and R. Abedi. Fracture modeling of rocks based on random field generation and simulation of inhomogeneous domains. In *Proceeding: 51th US Rock Mechanics/Geomechanics Symposium*, San Francisco, California, USA, 2017. ARMA 17-0643.

[33] CA Tang, LG Tham, PKK Lee, Y Tsui, and H Liu. Numerical studies of the influence of microstructure on rock failure in uniaxial compression - part II: constraint, slenderness, and size effect. *International Journal of Rock Mechanics and Mining Sciences*, 37(4):571–583, 2000.

[34] JG Teng, WC Zhu, and CA Tang. Mesomechanical model for concrete. part II: applications. *Magazine of Concrete Research*, 56(6):331–345, 2004.

[35] Gen Li and Chun-An Tang. A statistical meso-damage mechanical method for modeling trans-scale progressive failure process of rock. *International Journal of Rock Mechanics and Mining Sciences*, 74:133–150, 2015.

[36] Özge Dinç and Luc Scholtès. Discrete analysis of damage and shear banding in argillaceous rocks. *Rock Mechanics and Rock Engineering*, pages 1–18, 2017.

[37] Sachin Rangari, K Murali, and Arghya Deb. Effect of meso-structure on strength and size effect in concrete under compression. *Engineering Fracture Mechanics*, 2018.

[38] K.A. Acton, S.C. Baxter, B. Bahmani, P.L. Clarke, and R. Abedi. Voronoi tessellation based statistical volume element characterization for use in fracture modeling. *Computer Methods in Applied Mechanics and Engineering*, 2018. In Press.

[39] R. Abedi, R. B. Haber, S. Thite, and J. Erickson. An h–adaptive spacetime–discontinuous Galerkin method for linearized elastodynamics. *Revue Européenne de Mécanique Numérique (European Journal of Computational Mechanics)*, 15(6):619–42, 2006.